Timing and climate forcing of volcanic eruptions for the past 2,500 years

Sigl, M., Winstrup, M., McConnell, J. R., Welten, K. C., Plunkett, G., Ludlow, F., Büntgen, U., Caffee, M., Chellman, N., Dahl-Jensen, D., Fischer, H., Kipfstuhl, S., Kostick, C., Maselli, O. J., Mekhaldi, F., Mulvaney, R., Muscheler, R., Pasteris, D. R., Pilcher, J. R., ... Woodruff, T. E. (2015). Timing and climate forcing of volcanic eruptions for the past 2,500 years. *Nature*, *523*(7562), 543–549. https://doi.org/10.1038/nature14565

Published in:
Nature

Document Version:
Peer reviewed version

Timing and climate forcing of volcanic eruptions for the past 2,500 years

M. Sigl[1,2], M. Winstrup[3], J.R. McConnell[1], K.C. Welten[4], G. Plunkett[5], F. Ludlow[6], U. Büntgen[7,8,9], M. Caffee[10,11], N. Chellman[1], D. Dahl-Jensen[12], H. Fischer[8,13], S. Kipfstuhl[14], C. Kostick[15], O.J. Maselli[1], F. Mekhaldi[16], R. Mulvaney[17], R. Muscheler[16], D.R. Pasteris[1], J.R. Pilcher[5], M. Salzer[18], S. Schüpbach[8,13], J.P. Steffensen[12], B.M. Vinther[12], T.E. Woodruff[10]

[1] Desert Research Institute, Nevada System of Higher Education, Reno, NV 89512, USA

[2] now at Laboratory of Radiochemistry and Environmental Chemistry, Paul Scherrer Institut, 5232 Villigen, Switzerland

[3] Department of Earth and Space Sciences, University of Washington, Seattle, WA 98195, USA

[4] Space Sciences Laboratory, University of California, Berkeley, CA 94720, USA

[5] School of Geography, Archaeology & Palaeoecology, Queen's University Belfast, Belfast BT7 1NN, UK

[6] Yale Climate & Energy Institute, and Department of History, Yale University, New Haven, CT 06511, USA

[7] Swiss Federal Research Institute WSL, 8903 Birmensdorf, Switzerland

[8] Oeschger Centre for Climate Change Research, University of Bern, 3012 Bern, Switzerland

[9] Global Change Research Centre AS CR, 60300 Brno, Czech Republic

[10] Department of Physics, Purdue University, West Lafayette, IN 47907, USA

[11] Department of Earth, Atmospheric, and Planetary Sciences, Purdue University, West Lafayette, IN 47907, USA

[12] Centre for Ice and Climate, Niels Bohr Institute, University of Copenhagen, 2100 Copenhagen, Denmark

[13] Climate and Environmental Physics, University of Bern, 3012 Bern, Switzerland

[14] Alfred-Wegener-Institut Helmholtz-Zentrum für Polar- und Meeresforschung, 27570 Bremerhaven, Germany

[15] Department of History, The University of Nottingham, Nottingham NG7 2RD, UK

[16] Department of Geology, Quaternary Sciences, Lund University, 22362 Lund, Sweden

[17] British Antarctic Survey, Natural Environment Research Council, Cambridge, CB3 0ET, UK

[18] The Laboratory of Tree-Ring Research, University of Arizona, Tucson, AZ 85721, USA

Volcanic eruptions contribute to climate variability, but quantifying these contributions has been limited by inconsistencies in the timing of atmospheric volcanic aerosol loading determined from ice cores and subsequent cooling from climate proxies such as tree rings. Using new records of atmospheric aerosol loading developed from high-resolution, multi-parameter measurements from an array of Greenland and Antarctic ice cores as well as distinctive age markers to constrain chronologies, we resolve these inconsistencies. Here we show that large eruptions in the tropics and high latitudes were primary drivers of interannual-to-decadal temperature variability in the Northern Hemisphere during the past 2,500 years. Overall, cooling was proportional to the magnitude of volcanic forcing and persisted for up to ten years after some of the largest eruptive episodes. Our revised timescale now firmly implicates volcanic eruptions as catalysts in the major 6th century pandemics, famines, and socioeconomic disruptions in Eurasia and Mesoamerica while allowing multi-millennium quantification of climate response to volcanic forcing.

Volcanic eruptions are primary drivers of natural climate variability – as sulfate aerosol injections into the stratosphere shield the Earth's surface from incoming solar radiation, leading to short-term cooling at regional-to-global scales[1]. Temperatures during the past 2,000 years have been reconstructed at regional[2], continental[3], and global scales[4] using proxy information from natural archives. Tree-ring-based proxies provide the vast majority of climate records from mid- to high-latitude regions of (predominantly) the Northern Hemisphere (NH), whereas ice-core records (e.g., $\delta^{18}O$) represent both polar regions[3]. Climate forcing reconstructions for the Common Era (CE) – including solar (e.g., ^{10}Be)[5] and volcanic (e.g., sulfate)[6,7] activity – mostly derive from ice-core proxies. Any attempt to attribute reconstructed climate variability to external volcanic forcing – and distinguish between response, feedback, and internal variability of the climate system – requires ice-core chronologies that are synchronous with those of other climate reconstructions. In addition, multi-proxy climate reconstructions[2-4] derived from ice cores and other proxies such as tree rings will have diminished high-to-mid-frequency amplitudes if the individual climate records are on different timescales. Magnitudes and relative timing of simulated NH temperature response to large volcanic

eruptions are in disagreement with reconstructed temperatures obtained from tree rings[8,9], but it is unclear to what extent this model/data mismatch is caused by limitations in temperature reconstructions, volcanic reconstructions, or implementation of aerosol forcing in climate models[9-11]. The hypothesis of chronological errors in tree-ring-based temperature reconstructions[8,9] offered to explain this model/data mismatch has been tested and widely rejected[11-14], while new ice-core records have become available providing different eruption ages[15,16] and more precise estimates of atmospheric aerosol mass loading[17] than previous volcanic reconstructions. Using documented[18] and previous ice-core-based eruption ages[16], strong summer cooling following large volcanic eruptions has been recorded in tree-ring-based temperature reconstructions during the 2nd millennium CE with a one-to-two year lag similar to that observed in instrumental records after the 1991 Pinatubo eruption[19]. An apparent seven-year delayed cooling observed in individual tree-ring series relative to Greenland ice-core acidity peaks during the 1st millennium CE, however, suggests a bias in existing ice-core chronologies[20,21]. Using published ice-core chronologies, we also observed a seven-year offset between sulfate deposition in North Greenland and the start of tree-ring growth reduction in a composite of five multi-centennial tree-ring summer temperature reconstructions ("N-Tree") from the NH between 1 and 1000 CE (Methods), whereas tree-ring response was effectively immediate for eruptions occurring after 1250 CE (Fig. 1a).

Precise time marker across hemispheres. Independent age markers to test the accuracy of tree-ring and ice-core chronologies recently have become available with the detection of abrupt enrichment events in the ^{14}C content of tree rings. Rapid increases of atmospheric ^{14}C were first identified in individual growth increments of cedars from Japan between 774 and 775 CE[22] and between 993 and 994 CE[23]. The presence and timing of the event in 775 CE (henceforth, 775 event) has been reproduced by all radiocarbon measurements performed on tree rings at annual (or higher) resolution – including tree cores from Germany[24], the Alps[12], the Great Basin[25] (USA), and Siberia[25]. Recent identification of the same 775 CE event in kauri wood samples from New Zealand in the Southern Hemisphere (SH) demonstrates the global extent of the rapid ^{14}C increase and provides

81 further constraints on the event's exact timing (March 775 ± 6 months) due to the asynchronous SH
82 growing season[26]. While the cause of the 775 and 994 events is still debated[22,24,27], we expect that
83 they might also produce an excess of cosmogenic ^{10}Be through the interaction of high-energy
84 particles with atmospheric constituents[28,29]. Since both of these radionuclides are incorporated
85 rapidly into proxy archives via aerosol deposition (^{10}Be in ice cores) and photosynthesis ($^{14}CO_2$ in tree
86 rings), isotopic anomalies caused by these extraterrestrial events provide a global age marker to
87 directly link ice-core records to tree-ring chronologies[27]. The latter serve as an absolute and precise
88 age marker, verified (at least since 775 CE) by the coherence of the rapid increase in ^{14}C in all tree-
89 rings records for which high-resolution radiocarbon analyses were performed, including those
90 speculated to be at risk of missing rings[8]. We measured ^{10}Be concentrations at approximately annual
91 resolution in four ice cores – NEEM-2011-S1, TUNU2013, and NGRIP in Greenland, and the West
92 Antarctic Ice Sheet Divide Core (WDC) – over depth ranges encompassing the year 775 as dated in
93 existing ice-core chronologies in order to provide a direct, physically-based test of any dating bias in
94 these chronologies (Fig. 1, Extended Data Fig. 1, Methods, Supplementary Data S1). Both polar ice
95 sheets contain ^{10}Be concentrations exceeding the natural background concentration (>150%; 6σ) for
96 one-to-two consecutive years, compatible with the 775 CE event observed in tree rings. Using the
97 original ice-core age models[16,30], the ages of the ^{10}Be maxima in NEEM-2011-S1, NGRIP, and WDC are
98 768 CE, offset by 7 years from the tree-ring event. A further ^{10}Be anomaly measured in NEEM-2011-
99 S1 at 987 CE, compatible with the 994 CE event in tree rings, suggests a chronological offset was
100 present by the end of the first millennium CE (Fig. 1). Several different causes may have contributed
101 to the offset (see a summary in the Methods section), among which is the use of a previous dating
102 constraint[30] for Greenland where volcanic fallout in the ice was believed to indicate the historic (79
103 CE) eruption of Vesuvius.

104 **Revised ice-core chronologies.** Given the detection of a bias in existing ice-core chronologies, we
105 developed new timescales prior to the 1257 Samalas eruption[31] using highly resolved, multi-
106 parameter aerosol concentration records from three ice cores: NEEM-2011-S1, NEEM, and WDC. We

used the StratiCounter program, an automated, objective, annual-layer detection method based on Hidden Markov Model (HMM) algorithms[32] (Methods). For NEEM-2011-S1, obtained confidence intervals for the layer counts allowed us to improve the dating further by constraining the timescale using the 775 CE ^{10}Be anomaly and three precisely dated observations of post-volcanic aerosol loading of the atmosphere (Fig. 2, Extended Data Tables 1-3, Methods, Supplementary Data S2). We evaluated the accuracy of our new chronologies ("WD2014" for WDC and "NS1-2011" for NEEM) by comparison to (1) an extensive database of historical volcanic dust veil observations (Extended Data Fig. 2, Methods, Supplementary Data S2), (2) ice-core tephra evidence (Methods), and (3) the 994 CE event (Methods, Fig. 2). Using the new timescales, we found large sulfate signals in Greenland (e.g. 682, 574, 540 CE) between 500 and 2000 CE that frequently occurred within ±1 year from comparable – and independently dated – signals in Antarctica. These bipolar signals can now be confidently attributed to large tropical eruptions (Fig. 2). Back to 400 BCE, other large sulfate peaks (e.g., 44 BCE) were synchronous to within ±3 years (Fig. 2). We conclude that the revised ice-core timescales are accurate to within less than ±5 years during the past 2,500 years based on combined evidence from radionuclides, tree rings, tephra analyses, and historical accounts. Compared to the previous chronologies, age models differ prior to 1250 CE by up to 11 years (GICC05, Greenland) and 14 years (WDC06A-7, Antarctica) (Extended Data Fig. 3).

History of volcanic forcing. Employing our revised timescales and new high-resolution, ice-core sulfur measurements, we developed an extended reconstruction of volcanic aerosol deposition since early Roman times for both polar ice sheets from which we then estimated radiative forcing using established transfer functions[15] (Fig. 3, Methods, Supplementary Data S3-S5). This forcing series is characterized by improved dating accuracy, annual resolution, and a larger number of ice-core records in the Antarctic ice-core sulfate composite[17] than previous reconstructions[6,7]. It spans 2,500 years, allowing investigation of climate-volcano linkages more accurately and earlier than with previous reconstructions. It also provides a perspective on volcanic influences during major historical epochs, such as the growth of Roman imperial power and subsequent decline of the migration

period in Europe – times of (1) demographic and economic expansion as well as relative societal stability and (2) political turmoil and population instability, respectively[33]. With improved dating and lower volcanic-sulfate detection limits from the Antarctic array[17], we were able to detect, estimate, and attribute volcanic aerosol loading and forcing from 283 individual eruptive events during this period (Fig. 3). We attributed about 50% to mid-to-high latitudes NH sources, while 81 were attributed to tropical eruptions (having synchronous sulfate deposition on both polar ice sheets). These tropical volcanic eruptions contributed 64% of total volcanic forcing throughout the period, with five events exceeding the sulfate loading from Tambora, 1815 (Fig. 3, Extended Data Table 4). Events in 426 BCE and 44 BCE rival the great 1257 CE Samalas eruption (Indonesia) as the largest sulfate producing eruptions during this time. These two earlier events have not been widely regarded as large tropical eruptions with potential for strong climate impact[20], due to the lack of complete and synchronized sulfate records from Greenland and Antarctica. We base the claim that these two eruptions were tropical in origin and caused significant radiative perturbations on the observation that ice cores from Greenland and Antarctica record coeval (within their respective age uncertainties) and exceptionally high volcanic sulfate concentrations. Both these events were followed by strong and persistent growth reduction in tree-ring records[34] (Fig. 2) as typically observed after large tropical eruptions during the Common Era (Fig. 3).

Post-volcanic summer cooling. Superposed epoch analyses (Methods) performed on the "N-Tree" composite record centered on the largest volcanic signals between 500 BCE and 1250 CE as well as between 1250 and 2000 CE, show a clear post-volcanic cooling signal. For both periods, maximum tree-ring response lagged the date of initial increase of sulfate deposition by one year (Fig. 2), consistent with the response observed if using only historically documented eruptions with secure dating for the past 800 years[18]. The sharp and immediate (i.e., ≤1 year lag) response of tree growth to the ice-core volcanic signal throughout the past 2,500 years further corroborates the accuracy of our new ice-core timescales (Extended Data Fig. 4). Of the 16 most negative tree-growth anomalies (i.e., coldest summers) between 500 BCE and 1000 CE, 15 followed large volcanic signals – with the

four coldest (43 BCE, 536, 543, and 627 CE) occurring shortly after several of the largest events (Extended Data Tables 4, 5). Similarly, the coldest summers in Europe during the Common Era[3] were associated with large volcanic eruptions (Extended Data Table 5). Reduced tree growth after volcanic eruptions also was prominent in decadal averages of the "N-Tree" composite. All 16 decades with the most reduced tree growth for our 2,500-year period followed large eruptions (Fig. 3, Extended Data Table 5). In many cases, such as the coldest decade from 536 to 545 CE[3], sustained cooling was associated with the combined effect of several successive volcanic eruptions.

Strong post-volcanic cooling was not restricted to tropical eruptions; it also followed NH eruptions (Fig. 4), with maximum cooling in the year of volcanic-sulfate deposition. In contrast to the average of the 19 largest CE tropical eruptions, however, the NH-only eruptions did not give rise to any significant long-term cooling effect (Fig. 4). Persistence of implied post-volcanic cooling following the largest tropical eruptions is strongly expressed in temperature reconstructions based on tree-ring width measurements (e.g., those from the Alps), with recovery times of more than 10 years. Persistent cooling, with temperature reduction significantly below the pre-eruption baseline for six consecutive years, also is observed in temperature reconstructions based on maximum latewood density (e.g., those from Northern Scandinavia), the preferred proxy to quantify volcanic cooling contributions on climate due to less marked biological memory effects[35] (Fig. 4). These findings indicate that eruption-induced climate anomalies following large tropical eruptions may last longer than is indicated in many climate simulations (<3–5 years)[9,36,37] and that potential positive feedbacks initiated after large tropical eruptions (e.g., sea-ice feedbacks) may not be adequately represented in climate simulations[38,39]. The five-year averaged (lag 0 to lag 4 years) cooling response over three NH regions (Methods) following the 19 largest CE tropical eruptions was -0.6 ± 0.2 °C (2 standard error of the mean (SEM)), that of large NH eruptions was -0.4 ± 0.4 °C with strongest cooling induced in the high latitudes. Overall, cooling was proportional to the magnitude of volcanic forcing, with stratospheric sulfate loading exceeding that of Tambora inducing the strongest response of -1.1 ± 0.6 °C (Figs. 3, 4).

Global climate anomalies in 536-550 CE. Our new dating allowed us to clarify long-standing debates concerning the origin and consequences of the severe and apparently global climate anomalies observed from c.536–550 CE, which began with recognition of the "mystery cloud" of 536 CE[40] observed in the Mediterranean basin. Under previous ice-core dating, it has been argued that this dust veil corresponded to an unknown tropical eruption dated 533–534 CE (±2)[41]. Using our revised timescales, we found at least two large volcanic eruptions around this period (Fig. 5). A first – apparently NH, eruptive episode in 535 or early 536 CE – injected large amounts of sulfate and ash into the atmosphere. Geochemistry of tephra filtered from the NEEM-2011-S1 ice core at a depth corresponding to 536 CE indicated multiple North American volcanoes as likely candidates for a combined volcanic signal (Extended Data Fig. 5, Methods, Supplementary Data S5). Historical observations (Extended Data Table 3) identified atmospheric dimming as early as March 24, 536, lasting up to 18 months. The summer of 536 CE appeared exceptionally cold in all tree-ring reconstructions in the extra-tropical NH from N-America[34], over Europe[35,42,43] to Asia[44]. Depending upon reconstruction method, European summer temperatures in 536 CE dropped 1.6-2.5°C relative to the previous 30-year average[3]. A second eruptive episode in 539 or 540 CE, identified in both Greenland and Antarctica ice-core records and hence likely tropical in origin, resulted in up to 10% higher global aerosol loading than the Tambora 1815 eruption reconstructed from our bipolar sulfate records. Summer temperatures consequently dropped again, by 1.4-2.7°C in Europe in 541 CE[3], and cold temperatures persisted in the NH until almost 550 CE[3,33,34,42] (Figs. 2, 3, 5). This provides a notable environmental context to widespread famine and the great Justinian Plague 541-543 CE that was responsible for decimating populations in the Mediterranean and potentially China[45,46]. While certain climatic conditions (e.g., wet summers) have been linked to plague outbreaks in the past[47], a direct causal connection of these two large volcanic episodes and subsequent cooling to crop failures and outbreaks of famines and plagues is difficult to prove[33]. However, the exact delineation of two of the largest volcanic signals – with exceptionally strong and prolonged NH cooling; written evidence of famines and pandemics; as well as socio-economic

decline observed in Mesoamerica ("Maya Hiatus"[48]), Europe, and Asia – supports the idea that the latter may be causally associated with volcanically-induced climatic extremes.

Detailed study of major volcanic events during the 6th century (Fig. 5) and an assessment of post-volcanic cooling throughout the past 2,500 years using stacked tree-ring records and regional temperature reconstructions (Fig. 4, Extended Data Fig. 4) demonstrated that large eruptions in the tropics and high latitudes were primary drivers of interannual-to-decadal NH temperature variability. The new ice-core chronologies imply that previous multi-proxy reconstructions of temperature that include ice-core records[2-4] have diminished high-to-mid-frequency amplitudes and must be updated to accurately capture the timing and full amplitude of paleoclimatic variability. By creating a volcanic forcing index independent of but consistent with tree-ring-indicated cooling, we provide an essential step to advance understanding of external forcing on natural climate variability during the past 2,500 years. With the expected detection of additional rapid $\Delta^{14}C$ enrichment events from ongoing efforts in annual resolution ^{14}C tree-ring analyses[49], there will be future opportunities to further constrain ice-core dating throughout the Holocene and develop a framework of precisely dated, globally synchronized proxies of past climate variability and external climate forcing.

1 Robock, A. Volcanic eruptions and climate. *Rev Geophys* **45**, doi: 1029/2007rg000232 (2007).

2 Hanhijarvi, S., Tingley, M. P. & Korhola, A. Pairwise comparisons to reconstruct mean temperature in the Arctic Atlantic Region over the last 2,000 years. *Clim Dynam* **41**, 2039-2060 (2013).

3 PAGES 2k Consortium Continental-scale temperature variability during the past two millennia. *Nature Geoscience* **6**, doi: 10.1038/Ngeo1834 (2013).

4 Mann, M. E. *et al.* Proxy-based reconstructions of hemispheric and global surface temperature variations over the past two millennia. *P Natl Acad Sci USA* **105**, 13252-13257, (2008).

5 Usoskin, I. G. A history of solar activity over millenia. *Living Rev Sol. Phys* **10,** doi:10.12942/lrsp-2013-1 (2013).

6 Gao, C. C., Robock, A. & Ammann, C. Volcanic forcing of climate over the past 1500 years: An improved ice core-based index for climate models. *J Geophys Res-Atmos* **113**, doi: D23111 10.1029/2008jd010239 (2008).

7 Crowley, T. J. & Unterman, M. B. Technical details concerning development of a 1200-yr proxy index of global volcanism. *Earth System Science Data* **5,** 187-197 (2013).

8 Mann, M. E., Fuentes, J. D. & Rutherford, S. Underestimation of volcanic cooling in tree-ring-based reconstructions of hemispheric temperatures. *Nat Geosci* **5**, 202-205 (2012).

9 Mann, M. E., Rutherford, S., Schurer, A., Tett, S. F. B. & Fuentes, J. D. Discrepancies between the modeled and proxy-reconstructed response to volcanic forcing over the past millennium: Implications and possible mechanisms. *J Geophys Res-Atmos* **118**, 7617-7627 (2013).

10 Schurer, A. P., Hegerl, G. C., Mann, M. E., Tett, S. F. B. & Phipps, S. J. Separating Forced from Chaotic Climate Variability over the Past Millennium. *J Climate* **26**, 6954-6973 (2013).

11 Anchukaitis, K. J. *et al.* Tree rings and volcanic cooling. *Nat Geosci* **5**, 836-837 (2012).

12 Büntgen, U. *et al.* Extraterrestrial confirmation of tree-ring dating. *Nat Clim Change* **4**, 404-405 (2014).

13 Esper, J., Büntgen, U., Luterbacher, J. & Krusic, P. J. Testing the hypothesis of post-volcanic missing rings in temperature sensitive dendrochronological data. *Dendrochronologia* **31**, 216-222 (2013).

14 D'Arrigo, R., Wilson, R. & Anchukaitis, K. J. Volcanic cooling signal in tree ring temperature records for the past millennium. *J Geophys Res-Atmos* **118**, 9000-9010 (2013).

15 Plummer, C. T. *et al.* An independently dated 2000-yr volcanic record from Law Dome, East Antarctica, including a new perspective on the dating of the 1450s CE eruption of Kuwae, Vanuatu. *Clim Past* **8**, 1929-1940 (2012).

16 Sigl, M. *et al.* A new bipolar ice core record of volcanism from WAIS Divide and NEEM and implications for climate forcing of the last 2000 years. *J Geophys Res-Atmos* **118**, 1151-1169 (2013).

17 Sigl, M. *et al.* Insights from Antarctica on volcanic forcing during the Common Era. *Nat Clim Change* **4**, 693-697 (2014).

18 Esper, J. *et al.* European summer temperature response to annually dated volcanic eruptions over the past nine centuries. *B Volcanol* **75**, doi: 10.1007/S00445-013-0736-Z (2013).

19 Douglass, D. H. & Knox, R. S. Climate forcing by the volcanic eruption of Mount Pinatubo. *Geophys Res Lett* **32**, L05710, doi: 10.1029/2004gl022119 (2005).

20 Baillie, M. G. L. Proposed re-dating of the European ice core chronology by seven years prior to the 7th century AD. *Geophys Res Lett* **35**, L15813, doi: 10.1029/2008gl034755 (2008).

21 Baillie, M. G. L. & McAneney, J. Tree ring effects and ice core acidities clarify the volcanic record of the 1st millennium. *Clim. Past* **11**, 105-114 (2015).

22 Miyake, F., Nagaya, K., Masuda, K. & Nakamura, T. A signature of cosmic-ray increase in AD 774-775 from tree rings in Japan. *Nature* **486**, 240-242 (2012).

23 Miyake, F., Masuda, K. & Nakamura, T. Another rapid event in the carbon-14 content of tree rings. *Nat Commun* **4**, doi: 10.1038/Ncomms2783 (2013).

24 Usoskin, I. G. *et al.* The AD775 cosmic event revisited: the Sun is to blame. *Astron Astrophys* **552**, doi: 10.1051/0004-6361/201321080 (2013).

25 Jull, A. J. T. *et al.* Excursions in the 14C record at A. D. 774-775 in tree rings from Russia and America. *Geophys Res Lett* **41**, 3004-3010 (2014).

26 Güttler, D. *et al.* Rapid increase in cosmogenic 14C in AD 775 measured in New Zealand kauri trees indicates short-lived increase in 14C production spanning both hemispheres. *Earth Planet. Sci. Lett.* **411**, 290-297 (2015).

27 Miyake, F. *et al.* Cosmic ray event of AD 774-775 shown in quasi-annual 10 Be data from the Antarctic Dome Fuji ice core. *Geophys. Res. Lett.* **42**, 84-89 (2015).

28 Webber, W. R., Higbie, P. R. & McCracken, K. G. Production of the cosmogenic isotopes H-3, Be-7, Be-10, and Cl-36 in the Earth's atmosphere by solar and galactic cosmic rays. *J Geophys Res-Space* **112**, A10106, doi: 10.1029/2007ja012499 (2007).

29 Masarik, J. & Beer, J. An updated simulation of particle fluxes and cosmogenic nuclide production in the Earth's atmosphere. *J Geophys Res-Atmos* **114**, D11103, doi: 10.1029/2008jd010557 (2009).

30 Vinther, B. M. *et al.* A synchronized dating of three Greenland ice cores throughout the Holocene. *J Geophys Res-Atmos* **111**, D13102, doi: 10.1029/2005jd006921 (2006).

31 Lavigne, F. *et al.* Source of the great A.D. 1257 mystery eruption unveiled, Samalas volcano, Rinjani Volcanic Complex, Indonesia. *P Natl Acad Sci USA* **110**, 16742-16747 (2013).

32 Winstrup, M. *et al.* An automated approach for annual layer counting in ice cores. *Clim Past* **8**, 1881-1895 (2012).

33 McCormick, M. *et al.* Climate Change during and after the Roman Empire: Reconstructing the Past from Scientific and Historical Evidence. *J Interdiscipl Hist* **43**, 169-220 (2012).

34 Salzer, M. W. & Hughes, M. K. Bristlecone pine tree rings and volcanic eruptions over the last 5000 yr. *Quaternary Res* **67**, 57-68 (2007).

35 Esper, J., Duthorn, E., Krusic, P. J., Timonen, M. & Buntgen, U. Northern European summer temperature variations over the Common Era from integrated tree-ring density records. *J Quaternary Sci* **29**, 487-494 (2014).

36 Crowley, T. J. Causes of climate change over the past 1000 years. *Science* **289**, 270-277 (2000).

37 Driscoll, S., Bozzo, A., Gray, L. J., Robock, A. & Stenchikov, G. Coupled Model Intercomparison Project 5 (CMIP5) simulations of climate following volcanic eruptions. *J Geophys Res-Atmos* **117**, D17105, doi: 10.1029/2012jd017607 (2012).

38 Schneider, D. P., Ammann, C. M., Otto-Bliesner, B. L. & Kaufman, D. S. Climate response to large, high-latitude and low-latitude volcanic eruptions in the Community Climate System Model. *J Geophys Res-Atmos* **114**, D15101, doi: 10.1029/2008jd011222 (2009).

39 Zanchettin, D. *et al.* Inter-hemispheric asymmetry in the sea-ice response to volcanic forcing simulated by MPI-ESM (COSMOS-Mill). *Earth Syst Dynam* **5**, 223-242 (2014).

40 Stothers, R. B. Mystery Cloud of Ad-536. *Nature* **307**, 344-345 (1984).

41 Larsen, L. B. *et al.* New ice core evidence for a volcanic cause of the AD 536 dust veil. *Geophys Res Lett* **35**, L04708, doi: 10.1029/2007gl032450 (2008).

42 Büntgen, U. *et al.* 2500 Years of European Climate Variability and Human Susceptibility. *Science* **331**, 578-582 (2011).

43 Esper, J. *et al.* Orbital forcing of tree-ring data. *Nat Clim Change* **2**, 862-866 (2012).

44 D'Arrigo, R. *et al.* 1738 years of Mongolian temperature variability inferred from a tree-ring width chronology of Siberian pine. *Geophys Res Lett* **28**, 543-546 (2001).

45 Zhang, Z. B. *et al.* Periodic climate cooling enhanced natural disasters and wars in China during AD 10-1900. *P Roy Soc B-Biol Sci* **277**, 3745-3753 (2010).

46 Stothers, R. B. Volcanic dry fogs, climate cooling, and plague pandemics in Europe and the Middle East. *Climatic Change* **42**, 713-723 (1999).

47 Stenseth, N. C. *et al.* Plague dynamics are driven by climate variation. *P Natl Acad Sci USA* **103**, 13110-13115 (2006).

48 Dull, R. A. Evidence for forest clearance, agriculture, and human-induced erosion in Precolumbian El Salvador. *Ann Assoc Am Geogr* **97**, 127-141 (2007).

49 Taylor, R. E. & Southon, J. Reviewing the Mid-First Millennium BC C-14 "warp" using C-14/bristlecone pine data. *Nucl Instrum Meth B* **294**, 440-443 (2013).

Supplementary Information is available in the online version of the paper.

Acknowledgements. We thank the many persons involved in logistics, drill development and drilling, and ice-core processing and analysis in the field and our laboratories. This work was supported by the U.S. National Science Foundation (NSF). The authors appreciate support of the WAIS Divide Science Coordination Office (M. Twickler and J. Souney) for collection and distribution of the WAIS Divide ice core; Ice Drilling and Design and Operations (K. Dahnert) for drilling; the National Ice Core Laboratory (B. Bencivengo) for curating the core; Raytheon Polar Services (M. Kippenhan) for logistics support in Antarctica; and the 109th New York Air National Guard for airlift in Antarctica. NEEM is directed and organized by the Center of Ice and Climate at the Niels Bohr Institute and U.S. NSF, Office of Polar Programs. It is supported by funding agencies and institutions in Belgium (FNRS-CFB and FWO), Canada (NRCan/GSC), China (CAS), Denmark (FIST), France (IPEV, CNRS/INSU, CEA and ANR), Germany (AWI), Iceland (RannIs), Japan (NIPR), Korea (KOPRI), The Netherlands (NWO/ALW), Sweden (VR), Switzerland (SNF), United Kingdom (NERC), and the USA (U.S. NSF, Office of Polar Programs). We thank B. Nolan, O. Amir, K. D. Pang, M. McCormick, A. Matthews, and B. Rossignol for assistance in surveying and/or interpreting the historical evidence. We thank S. Kuehn for commenting on possible correlations for the tephra. A. Aldahan and G. Possnert are thanked for their support in the NGRIP ^{10}Be preparations and measurements at the Department of Earth Sciences and the Tandem laboratory at Uppsala University. We gratefully acknowledge R. Kreidberg for his editorial advice.

The following individual grants supported this work: NSF/OPP grants 0839093, 0968391, and 1142166 to J.R.M. for development of the Antarctic ice core records and NSF/OPP grants 0909541, 1023672, and 1204176 to J.R.M. for development of the Arctic ice core records. M.W. was funded by the Villum Foundation. K.C.W. was funded by NSF/OPP grants 0636964 and 0839137. M.W.C. and T.W. were funded by NSF/OPP grants 0839042 and 0636815. F.L. was funded by the Yale Climate & Energy Institute, Initiative for the Science of the Human Past at Harvard, and Rachel Carson Center for Environment and Society of the Ludwig-Maximilians-Universität (LMU Munich). C.K. was funded by a Marie Curie FP7 Integration Grant within the 7th European Union Framework Programme. M.

361 Sa. was funded by NSF grant ATM 1203749. R.M. was funded by the Swedish Research Council
362 (DNR2013-8421). The division of Climate and Environmental Physics, Physics Institute, University of
363 Bern, acknowledges financial support by the SNF and the Oeschger Centre.

364 **Author Contributions.** M.Si. designed the study with input from J.R.M., M.W., G.P., and F.L. The
365 manuscript was written by M.Si., M.W., F.L., and J.R.M., with contributions from K.C.W., G.P., U.B.,
366 B.V. in interpretation of the measurements. Ice-core chemistry measurements were performed by
367 J.R.M., M.Si., O.J.M., N.C., D.R.P. (NEEM, B40, TUNU2013), and by S.S., H.F., R.Mul. (NEEM). K.C.W.,
368 T.E.W., and M.C. completed ice core ^{10}Be measurements. F.M. and R.Mus. were responsible for the
369 NGRIP ice core ^{10}Be measurements. M.Si., M.W., B.V., and J.R.M. analyzed ice-core data and
370 developed age models. F.L. and C.K. analyzed historical documentary data. G.P and J.R.P. performed
371 ice-core tephra analysis and data interpretation. U.B. and M.Sa. contributed tree-ring data. D.D.-J.,
372 B.V., J.P.S., S.K., and O.J.M. were involved in drilling of the NEEM ice core. TUNU2013 was drilled by
373 M.Si., N.C. and O.J.M., and the B40 ice core was drilled by S.K. and made available for chemistry
374 measurements. D.D.-J. and J.P.S. were responsible for NEEM project management, sample
375 distribution, logistics support, and management. All authors contributed toward improving the final
376 manuscript.

377 **Author Information.** The authors declare no competing financial interests. Correspondence and
378 requests for materials should be addressed to J.R.M. (Joe.McConnell@dri.edu).

379 **Figure 1 | Annual ^{10}Be ice-core records and post-volcanic cooling from tree rings under existing ice-**
380 **core chronologies. a)** Superposed epoch analysis for the seven largest volcanic signals in NEEM-
381 2011-S1 between 78 and 1000 CE and for the 10 largest eruptions between 1250 and 2000 CE,
382 respectively[16]. Shown are growth anomalies from a multi-centennial, temperature-sensitive tree-ring
383 composite (N-Tree[42,43,76-78], Methods) 10 years after the year of volcanic sulfate deposition at NEEM
384 ice core site in Greenland (GICC05 timescale), relative to the level five years prior to sulfate
385 deposition; **b)** annually resolved ^{10}Be concentration records from WDC, TUNU2013, NGRIP, and

386 NEEM-2011-S1 ice cores on their original timescales and annually resolved $\Delta^{14}C$ series from tree-ring
387 records between 755-795 CE[22,24], with arrows representing the suggested time shifts for
388 synchronization; error bars are 1σ measurement uncertainties; estimated relative age uncertainty
389 for TUNU2013 at this depth interval from volcanic synchronization with NEEM-2011-S1 is ±1 year; **c)**
390 annually resolved ^{10}Be concentration record from NEEM-2011-S1 ice core on its original timescale
391 and annually resolved $\Delta^{14}C$ series from tree rings between 980-1010 CE[23]; error bars are 1σ
392 measurement uncertainties.

393 **Figure 2 | Re-dated ice-core, non-sea-salt sulfur records from Greenland and Antarctica in relation**
394 **to growth anomalies in the N-Tree composite. a)** Upper panel: Ice-core, non-sea-salt sulfur (nssS)
395 records from Greenland (NEEM, NEEM-2011-S1) on the NS1-2011 timescale between 500 BCE and
396 1300 CE, with identified layer of Tianchi tephra[67] highlighted (orange star). Calendar years are given
397 for the start of volcanic sulfate deposition. Events used as fixed age markers to constrain the dating
398 (i.e., 536, 626, 775, 939, and 1258) are indicated (purple stars). Annually resolved ^{10}Be concentration
399 record (green) from NEEM-2011-S1 encompassing the two $\Delta^{14}C$ excursion events in trees from 775
400 and 994; middle panel: tree-ring growth anomalies (relative to 1000-1099 CE) for the N-Tree
401 composite[42,43,76-78]; lower panel: nssS records from Antarctica (WDC, B40) on the WD2014 timescale
402 and annually resolved ^{10}Be concentrations from WDC; **b**) superposed epoch analysis for 28 large
403 volcanic signals during the past 2,500 years. Tree-ring growth anomalies relative to the timing of
404 reconstructed sulfate deposition in Greenland (NS1-2011) are shown for 1250 to 2000 CE and 500
405 BCE to 1250 CE.

406 **Figure 3 | Global volcanic aerosol forcing and NH temperature variations for the past 2,500 years.**
407 **a)** 2,500 year record of tree-growth anomalies (N-Tree[42,43,76-78]; relative to 1000-1099 CE) and
408 reconstructed summer temperature anomalies for Europe and Arctic[3] ; 40 coldest single years and
409 12 coldest decades based on N-Tree are indicated; **b**) reconstructed global volcanic aerosol forcing
410 from bipolar sulfate composite records from tropical (bipolar), NH, and SH eruptions. Total (i.e., time

411 integrated) forcing values are calculated by summing the annual values for the duration of volcanic
412 sulfur deposition. 40 largest volcanic signals are indicated, and ages are given for events
413 representing atmospheric sulfate loading exceeding Tambora 1815.

414 **Figure 4 | Post-volcanic cooling.** Superposed composites (time segments from selected periods in
415 the Common Era positioned so that the years with peak negative forcing are aligned) of the JJA
416 temperature response to: **a)-c)** 24 largest eruptions (>Pinatubo 1991) for three regional
417 reconstructions in Europe[3,35,42]; **d)-f)** 19 largest tropical eruptions; **g)** five largest NH eruptions; **h)**
418 eruptions with negative forcing larger than Tambora 1815 for Northern Europe and **i)** for Central
419 Europe (note the different scale for g-i); shown are JJA temperature anomalies (°C) for 15 years after
420 reconstructed volcanic peak forcing, relative to the five years before the volcanic eruption. Dashed
421 lines present two times the standard error of the mean (2 SEM) of the temperature anomalies
422 associated with the multiple eruptions. 5-year average post-volcanic temperatures are shown for
423 each reconstruction (lag 0 to lag +4 yrs, gray shading).

424 **Figure 5 | Volcanism and temperature variability during the Migration Period (500-705 CE).** Upper
425 panel: Ice-core non-sea-salt sulfur (nssS) records from Greenland (NEEM-2011-S1, TUNU2013).
426 Insets give translations of historical documents describing observation of post-volcanic atmospheric
427 effects in 536-537 and 626-627 CE. Calendar years for five large eruptions are given for the start of
428 volcanic sulfate deposition; middle panel: Summer temperature anomalies for Europe[3], and
429 reconstructed N-Tree growth anomalies and occurrence of frost rings in North American bristlecone
430 pine tree-ring records; lower panel: nssS records from Antarctica (WDC, B40) on the WD2014
431 timescale; attribution of the sulfur signals to bipolar, NH, and SH events based on the timing of
432 deposition on the two independent timescales is indicated by shading.

433 **Methods**

434 **Ice cores.** This study included new and previously described ice-core records from five drilling sites
435 (Extended Data Fig. 1, Supplementary Data S1). The upper 577 m of the 3,405 m WAIS Divide (WDC)

436 core from central West Antarctica and a 410 m intermediate-length core (NEEM-2011-S1) drilled in
437 2011 close to the 2,540 m North Greenland Eemian Ice Drilling (NEEM)[50] ice core previously have
438 been used to reconstruct sulfate deposition in both polar ice sheets[16]. These coring sites are
439 characterized by relatively high snowfall (~200 kg m^{-2} yr^{-1}) and have comparable elevation, latitude,
440 and deposition regimes. WDC and NEEM-2011-S1 provided high-resolution records that allowed
441 annual-layer dating based on seasonally varying impurity content[16]. New ice-core analyses included
442 the upper 514 m of the main NEEM core used to extend the record of NEEM-2011-S1 to cover the
443 past 2,500 years, as well as B40 drilled in 2012 in Dronning Maud Land in East Antarctica and
444 TUNU2013 drilled in 2013 in Northeast Greenland – both characterized by lower snowfall rates (~70-
445 100 kg m^{-2} yr^{-1}). Volcanic sulfate concentration from B40 had been reported previously for the past
446 2,000 years[17], but we extended measurements to 200 m depth to cover the past 2,500 years.

447 **High-resolution, ice-core aerosol analyses.** Ice-core analyses were performed at the Desert
448 Research Institute (DRI) using 55 to 100 cm long, longitudinal ice core sections (33 x 33 mm wide).
449 The analytical system for continuous analysis included two Element2 (Thermo Scientific) high-
450 resolution inductively coupled plasma mass spectrometers (HR-ICP-MS) operating in parallel for
451 measurement of a broad range of ~35 elements; an SP2 (Droplet Measurement Technologies)
452 instrument for black carbon (BC) measurements; and a host of fluorimeters and spectrophotometers
453 for ammonium (NH_4^+), nitrate (NO_3^-), hydrogen peroxide (H_2O_2), and other chemical species. All
454 measurements were exactly co-registered in depth, with depth resolution typically less than 10-15
455 mm[51-53]. We corrected total sulfur (S) concentrations for the sea-salt-sulfur contribution using sea-
456 salt-Na concentrations[16]. Measurements included TUNU2013 and NEEM (400-515 m) in Greenland,
457 and B40 in Antarctica (Extended Data Fig. 1). Gaps (i.e., ice not allocated to DRI) in the high-
458 resolution sulfur data of the NEEM core were filled with ~4 cm resolution discrete sulfate
459 measurements using fast ion-chromatography techniques[54] performed in the field between 428 and
460 506 m depth.

461 Independent analyses of the upper part of the NEEM main core were performed in the field
462 using a continuous flow analysis (CFA) system[55] recently modified to include a new melter head
463 design[56]. Ca^{2+}, NH_4^+, and H_2O_2 were analyzed by fluorescence spectroscopy; Na^+ and NO_3^- by
464 absorption spectroscopy; conductivity of the meltwater by a micro flow cell (Amber Science Inc.);
465 and a particle detector (Abakus, Klotz) was used for measuring insoluble dust particle concentrations
466 and size distribution[57]. Effective depth resolution typically was better than 20 mm. Measurements
467 were exactly synchronized in depth using a multicomponent standard solution; the accuracy of the
468 depth assignment for all measurements typically was better than 5 mm.

469 **High-resolution measurements of ^{10}Be in ice cores using accelerator mass spectrometry (AMS).**
470 Samples from the NEEM-2011-S1, WDC, NGRIP, and TUNU2013 ice cores encompassing the time
471 period of the Δ^{14}C anomalies from tree-ring records[12,22-25] were used for ^{10}Be analysis
472 (Supplementary Data S1). NEEM-2011-S1 and WDC were sampled in exact annual resolution, using
473 the maxima (minima in WDC) of the annual cycles of Na concentrations to define the beginning of
474 the calendar year[16]. NGRIP was sampled at a constant resolution of 18.3 cm providing an age
475 resolution of about one year. Similarly, TUNU2013 was sampled in quasi-annual resolution according
476 to the average annual-layer thickness expected at this depth based on prior volcanic synchronization
477 to NEEM-2011-S1. The relative age uncertainty for TUNU2013 with respect to the dependent NEEM-
478 2011-S1 chronology at this depth is assumed to be ±1 year at most given a distinctive match for
479 selected volcanic trace elements in both ice core records (752-764 CE, NS1-2011 timescale). Sample
480 masses ranged between 100 and 450 g, resulting in median overall quantification uncertainties of
481 less than 4–7%. The ^{10}Be/^{9}Be ratios of samples and blanks were measured relative to well-
482 documented ^{10}Be standards[13] by AMS at Purdue's PRIME laboratory (WDC, NEEM-2011-S1,
483 Tunu2013) and Uppsala University (NGRIP)[58,59]. Results were corrected for an average blank ^{10}Be/^{9}Be
484 ratio, corresponding to corrections of 2–10% of the measured ^{10}Be/^{9}Be ratios.

485 **Annual-layer dating using the StratiCounter algorithm.** For annual-layer interpretation, we used
486 DRI's broad-spectrum aerosol concentration data from WDC (188–577 m), NEEM-2011-S1 (183–411

487 m), and NEEM (410–515 m), as well as NEEM aerosol concentration data (183–514 m) from the field-
488 based CFA system. The original timescale for NEEM-2011-S1 was based on volcanic synchronization
489 to the NGRIP sulfate record on the GICC05 timescale and annual-layer interpretation between the
490 volcanic age markers, while WDC previously was dated by annual-layer counting[16].

491 Parameters with strong intra-annual variability included tracers of sea salt (e.g., Na, Cl, Sr),
492 dust (e.g., Ce, Mg, insoluble particle concentration), and marine biogenic emissions such as non-sea-
493 salt sulfur (nssS). Tracers of biomass-burning emissions, such as BC, NH_4^+, and NO_3^-, also showed
494 strong seasonal variations in deposition during pre-industrial times[16,60,61]. Datasets used for annual
495 layer interpretation are provided in Extended Data Table 1. For NEEM-2011-S1, the final database
496 used for annual-layer dating included 13 parameters and the ratio of nssS/Na. For WDC, the final
497 database included five parameters and the ratio of nssS/Na. For NEEM (410-515 m depth), the final
498 database included eight parameters (Na^+, Ca^{2+}, NH_4^+, H_2O_2, NO_3^-, conductivity, insoluble particle
499 concentrations, and ECM[62]) from the field-based measurements and eleven parameters (Na, Cl, Mg,
500 Mn, Sr, nssS, nssS/Na, nssCa, BC, NO_3^-, NH_4^+) from the DRI system.

501 We focused here on the time period prior to the large volcanic eruption of Samalas in 1257
502 CE[31], clearly detectable as an acidic peak in both ice-core records, and consequently started annual-
503 layer counting of NEEM-2011-S1, NEEM, and WDC at the depth of the corresponding sulfur signal.
504 For the time period 1257 CE to present, ice-core chronologies were constrained by numerous
505 historic eruptions and large sulfate peaks showing a strong association to Northern Hemisphere (NH)
506 cooling events as indicated by tree-ring records[16].

507 We applied the StratiCounter layer-detection algorithm[32] to the multi-parameter aerosol
508 concentration records (n=14 for NEEM-2011-S1; n=6 for WDC; n=8 for NEEM <410 m; n=19 for NEEM
509 >410 m) to objectively determine the most likely number of annual layers in the ice cores along with
510 corresponding uncertainties. The StratiCounter algorithm is based on statistical inference in Hidden
511 Markov Models (HMMs), and it determines the maximum likelihood solution based on the annual

512 signal in all aerosol records in parallel. Some of these displayed a high degree of similarity, so we
513 weighted these records correspondingly lower. The algorithm was run step-wise down the core,
514 each batch covering approximately 50 years, with a slight overlap. All parameters for the statistical
515 description of a mean layer and its inter-annual variability in the various aerosol records were
516 determined independently for each batch as the maximum likelihood solution. The algorithm
517 simultaneously computes confidence intervals for the number of layers within given sections,
518 allowing us to provide uncertainty bounds on the number of layers between selected age-marker
519 horizons (Extended Data Table 2).

520 Annual-layer detection in the NEEM main core below 410 m was made more difficult by
521 frequent occurrence of small gaps in the two independent high-resolution aerosol data sets.
522 Depending on the parameter, data gaps from the CFA field measurements accounted for up to 20%
523 of the depth range between 410 and 515 m, but the combined aerosol records from both analyses
524 provided an almost complete aerosol record with 96% data coverage. As this was the first time that
525 the StratiCounter algorithm was used simultaneously on data records from two different melt
526 systems, with different characteristics and lack of exact co-registration, we also manually
527 determined annual layers below 410 m using the following approaches: one investigator used Na
528 and nssCa concentrations and the ratio of nssS/Na (from DRI analysis) as well as Na^+ and insoluble
529 particle concentrations (from CFA analysis) as primary dating parameters. BC, NH_4^+, nssS, and
530 conductivity were used as secondary dating parameters where annual-layer interpretation was
531 ambiguous. A second investigator used DRI's Na, Ca, BC, NH_4^+ and CFA Na^+, Ca^{2+}, and NH_4^+
532 measurements as parameters. The annual-layer interpretation of the NEEM core between 410 and
533 514 m from investigator 1 was within the interpretation uncertainties of the StratiCounter output,
534 from which it differed less than a single year over the majority of this section, and it differed from
535 independently counted timescales (e.g., GICC05)[62] by on average less than three years (Extended
536 Data Fig. 2). This set of layer counts was used for the resulting timescale.

New ice-core chronologies (NS1-2011, WD2014). We defined the depth of NEEM-2011-S1 containing the maximum ^{10}Be concentration as the year 775 CE. Relative to this constraint, the maximum likelihood ages for three large volcanic sulfate peaks were within ±1 year of documented historical reports from early written sources of prominent and sustained atmospheric dimming observed in Europe and/or the Near East (Extended Data Table 3, Supplementary Data S2). Automated-layer identification for NEEM-2011-S1 was therefore constrained by tying the respective ice-core volcanic signals to the corresponding absolute historically-dated ages of 536, 626, and 939 CE (Extended Data Table 2) – thereby creating a new ice-core timescale (NS1-2011). The volcanic sulfur signal corresponding to the eruption of Samalas believed to have occurred in late 1257[31] was constrained to 1258 CE to account for several months' delay in sulfate deposition in the high latitudes. Before 86 CE (the bottom depth of NEEM-2011-S1), the NS1-2011 timescale was extended using the manually-derived annual-layer interpretation of the combined NEEM aerosol data-sets back to 500 BCE (Fig. 2).

In NS1-2011 we did not attribute acid layers to the historical eruptions Vesuvius 79 and Hekla 1104, due to a lack of corroborative tephra at these depths in this and a previous study[63]. Possible Vesuvian tephra was reported from the Greenland Ice Sheet Project (GRIP) ice core at 429.3 m depth[64], but in view of the new annual-layer dating results (Extended Data Fig. 3), we concluded that this layer dates to 87/88 CE. Furthermore, volcanic sulfate deposition values for the corresponding event show a strong spatial gradient over Greenland with highest values in NW Greenland[16] and lowest in Central and South Greenland[65], favoring the attribution of a volcanic source from the high latitudes. Documentary sources (Supplementary Data S2) also suggest that the main vector of ash transport following the Vesuvius 79 CE eruption was toward the eastern Mediterranean[66].

For WDC, we do not have other sufficiently well-determined age constraints besides the rapid ^{10}Be increase in 775 CE and the sulfur signal of the Samalas 1257 eruption. Therefore, no

562 additional constraints were used when creating the new ice-core timescale ("WD2014") from the
563 StratiCounter annual-layer interpretation back to 396 BCE.

564 Depth-age information for six distinctive marker horizons in Greenland is given, and five of
565 these horizons were used to constrain NS1-2011 (Extended Data Table 3). Similarly, depth
566 information, the number of annual layers, and 95% confidence intervals between distinctive volcanic
567 marker horizons are given for NEEM, NEEM-2011-S1, and WDC, supporting attribution of these ice-
568 core signals to eruptions in the low latitudes with bipolar sulfate deposition.

569 **Evaluation of NS1-2011 using independent age information.** We evaluated timescale accuracy using
570 additional distinctive age markers not used during chronology development:

571 1) Tephra from the eruption of Changbaishan/Tianchi (China)[67] was detected in NEEM-2011-S1
572 in 946–947 CE, in agreement with widespread documentary evidence of an eruption in that
573 region in winter 946/47 CE[68]also supported by a high-precision ^{14}C wiggle-match age of 946 ±
574 3 CE obtained from a tree killed during this eruption[68].
575 2) The rapid increase of ^{10}Be from the 994 event occurred in NEEM-2011-S1 in 993 CE,
576 consistent with $\Delta^{14}C$ from Japanese tree rings showing that the rapid increase in
577 radionuclide production took place between the NH growing seasons of 993 and 994 CE[23].
578 3) To assess the accuracy of the NS1-2011 timescale prior to the earliest age marker at 536 CE,
579 we compiled an independent time series of validation points, featuring years with well dated
580 historical reports of atmospheric phenomena associated with high-altitude volcanic dust
581 and/or aerosols (Supplementary Data S2) as known from modern observations to occur after
582 major eruptions (e.g., Krakatau, 1883). These phenomena include diminished sunlight,
583 discoloration of the solar disk, solar coronae (i.e., Bishop's Rings), and deeply red twilights
584 (i.e., volcanic sunsets)[69,70]. Thirty-two events met our criteria as validation points for the pre-
585 536 CE NS1-2011 timescale. For the earliest in 255 BCE, it was reported in Babylon that "the
586 disk of the sun looked like that of the moon"[73]. For the latest in 501 CE, it was reported in

North China that "the Sun was red and without brilliance"[74]. We found that NEEM volcanic event years (including both NEEM and NEEM-2011-S1 data) occurred closely in time (i.e., within a conservative ±3 year margin) to 24 (75.0%) of our validation points (Extended Data Figure 2). To assess whether this association arose solely by chance, we conducted a Monte Carlo equal means test with 1,000,000 iterations (Supplementary Data S2) and found that the number of volcanic event years within ±3 years of our validation points was significantly greater than expected randomly ($p<0.001$). A significant association was also observed ($p<0.001$) when using less conservative error margins (±1 and ±2 years) and when excluding any historical observations with less certainty of a volcanic origin (Supplementary Data S2). When placing volcanic event years on the original GICC05 timescale, we did not observe any statistically significant association with our independent validation points.

Potential causes of a previous ice-core dating bias. Interpretation of annual layers in ice cores is subject to accumulating age uncertainty due to ambiguities in the underlying ice-core profiles[30,73]. Bias in existing chronologies may arise from several factors, including: 1) low effective resolution of some ice core measurements (NGRIP, GRIP); 2) use of only single (or few) parameters for annual-layer interpretation (GRIP, Dye-3); 3) intra-annual variations in various ice-core parameters falsely interpreted as layer boundaries (e.g., caused by summer melt in Dye-3)[74]; 4) use of tephra believed to originate from the 79 CE Vesuvian eruption[64] as a fixed reference horizon to constrain the Greenland ice-core dating[30]; 5) use of manual-layer interpretation techniques that may favor interpretations consistent with *a priori* knowledge or existing chronologies (WDC)[16,21].

Volcanic synchronization of B40, TUNU2013, and NGRIP to WDC and NEEM. Two high-resolution sulfur ice-core records (TUNU2013, Greenland and B40, Antarctica) were synchronized to NEEM-2011-S1 and WDC, respectively, using volcanic stratigraphic age markers[17] with relative age uncertainty between the tie-points estimated to not exceed ±2 years. The NGRIP sulfate record measured at 5 cm depth resolution[15] similarly was synchronized to NS1-2011 using 124 volcanic tie-points between 226 and 1999 CE. During the time period with no sulfur record yet available for WDC

(before 396 BCE), a tentative chronology for B40 was derived by linearly extrapolating mean annual-layer thickness for B40 as derived from the synchronization to WDC between the earliest volcanic match points.

2,500 year global volcanic forcing ice-core index. We constructed an index of global volcanic aerosol forcing by (1) re-dating and extending to 500 BCE an existing reconstruction of sulfate flux from an Antarctic ice-core array[17] by applying an area weighting of 80/20 between East Antarctica and West Antarctica to B40 and WDC volcanic sulfate flux values, respectively; (2) compositing NGRIP and the NEEM-2011-S1/NEEM sulfate flux records to a similar Greenland sulfate deposition composite back to 500 BCE; (3) using established scaling functions[6,75] to estimate hemispheric sulfate aerosol loading from both polar ice-core composites; and (4) scaling global aerosol loading to the total (i.e., time integrated) radiative volcanic aerosol forcing following the Tambora 1815 eruption[7]. Since the NS1-2011 and WD2014 timescales are independent of each other, the timing of bipolar events had to be adjusted to follow a single timescale to derive a unified global volcanic forcing series. We chose NS1-2011 as the reference chronology for most of the volcanic time series because this age model was constrained and validated by more stratigraphic age markers than WD2014. WD2014 was used as the reference chronology only between 150 and 450 CE, because of better data quality during that time period. TUNU2013 was not included in the Greenland ice-core composite because annual-layer thickness variability at this site is influenced strongly by glaciological processes, leading to relatively large uncertainties in atmospheric sulfur-deposition determinations.

NH tree-ring composite. Tree-ring records from certain locations reflect summer cooling (as is widespread observed after volcanic eruptions) with no age uncertainty in annual ring-width dating, thus allowing independent validation of ice-core timescales and the derived volcanic forcing indices. However, no tree-ring-based temperature reconstructions of large spatial scales span the full 2,500 years represented by our new ice-core chronologies. To thus evaluate our new ice-core chronologies and assess the consistency of response throughout the past 2,500 years, we compiled a composite

(entitled “N-Tree”) of multi-centennial tree growth records at locations where temperature is the limiting growth factor. We selected available NH tree-ring records that provided a continuous record of >1,500 years and showed a significant positive relationship with JJA temperatures during the instrumental period (1901–2000 CE) with $p<0.005$ (adjusted for a reduced sample size due to autocorrelation of the datasets). In total, five tree-ring chronologies (three based on ring-width measurements, two based on measurements of maximum latewood density) met these criteria[42,43,76-78] of which three are located in the high-latitudes of Eurasia (Extended Data Figure 1).

As various climatic and non-climatic parameters may influence sensitivity of tree growth to temperatures during the 20th century[79-81], we used the time period 1000-1099 CE as a common baseline for standardizing tree growth anomalies among the five chronologies and built a tree growth composite record “N-Tree” (z-scores) by averaging the individual records. Correlations between “N-Tree” (N=5) and the average of three regional reconstructions for the Arctic, Europe, and Asia (N>275)[3] between 1800 and 2000 CE are very high ($r = 0.86$, N=201, $p<0.0001$), suggesting that much of the large-scale variation in temperature is explained by these selected tree-ring records. Three records in “N-Tree” cover the period from 138 BCE to the present, thus allowing at least a qualitative assessment of the coherence of growth reduction following large volcanic eruptions prior to the Common Era (Fig. 2, Extended Data Fig. 4).

Temperature reconstructions. To quantify the CE climate impact and investigate regional differences, we used tree-ring-based JJA temperature reconstructions covering the past 2,000 years with demonstrated strong relationship ($r \geq 0.45$; $p<0.0001$; Extended Data Fig. 1) to instrumental JJA temperature data[82] between 1901 and 2000. For regions where this criterion was met by several reconstructions (e.g., Scandinavia), we limited the analysis to the most recently updated reconstruction[35]. Three regional reconstructions from Central Europe [42], Northern Europe[35], and Northern Siberia (Yamal, not shown)[76] as well as a continental-scale reconstruction for Europe[3] met this criterion and were used to quantify the average response of summer temperature to volcanic forcing during the Common Era (Figs. 3, 4).

Superposed epoch analyses. To assess tree-ring growth reduction and summer cooling following large eruptions, we used superposed epoch analyses[83,84]. We selected all volcanic eruptions (28 events in total, 24 CE events) with time-integrated volcanic forcing greater than -7.5 W m^{-2} (i.e., eruptions larger than Pinatubo 1991) and aligned the individual segments of "N-Tree" and regional JJA temperature reconstructions relative to ice-core-indicated peak forcing. Composite response was calculated for the average of the individual series (lag 0 to lag 10 or 15 years) relative to the average values five years prior to individual volcanic events (lag -5 to lag -1 year). 95% confidence intervals represent 2 SEM of the tree-growth (Extended Data Figure 4) and temperature anomalies (Figure 4) associated with the multiple eruptions.

Cryptotephra analyses of the 536 CE sample from NEEM-2011-S1. We analyzed samples from NEEM-2011-S1 for tephra between 326.73 and 328.06 m depth, corresponding to 531–539 CE (NS1-2011 timescale). Samples (200 to 500 g) were filtered, and elemental composition of recovered volcanic glass shards determined by electron microprobe analysis (EPMA) at Queen's University Belfast using established protocols[63,67,85] and secondary glass standards[86,87]. Between 326.73 and 327.25 m, large volume samples were cut at 8 cm depth resolution (≤0.5 yr) and with an average cross section of 26 cm^2. Between 327.25 and 328.06 m, the average cross section was 7 cm^2 and depth resolution 20 cm (~1 yr resolution). Tephra particles (n ≥17) were isolated from a sample of ice (327.17–327.25 m depth, 251 g) corresponding to the sulfate spike at 536 CE. The glass shards were heterogeneous in size (20–80 μm), morphology (platey, blocky, vesicular, microlitic), and geochemistry (andesitic, trachytic, rhyolitic). Individual shards had geochemical compositions that share affinities with volcanic systems in the Aleutian arc (Alaska)[88], Northern Cordilleran volcanic province (British Columbia)[89], and Mono-Inyo Craters area (California)[90,91] – indicating at least three synchronous eruptive events, all situated in western North America between 38 and 58°N (Extended Data Fig. 5; Supplementary Data S5).

Data: Ice-core data (chemistry, including sulfur; ^{10}Be), resulting timescales, and the volcanic forcing reconstruction are provided as online supplementary material (Supplementary Data S1, S3-S5); Historical documentary data is provided as Supplementary Data S2. The code for the StratiCounter program is accessible at the github repository (http://www.github.com/maiwinstrup/StratiCounter); NGRIP SO_4 data can be obtained at http://www.iceandclimate.nbi.ku.dk/data/2012-12-03_NGRIP_SO4_5cm_Plummet_et_al_CP_2012.txt ; tree-ring records and temperature reconstructions are from Pages-2k Consortium (Database S1, S2) (http://www.nature.com/ngeo/journal/v6/n5/full/ngeo1797.html#supplementary-information).

References

50 Dahl-Jensen, D. *et al.* Eemian interglacial reconstructed from a Greenland folded ice core. *Nature* **493**, 489-494 (2013).

51 McConnell, J. R. Continuous ice-core chemical analyses using inductively Coupled Plasma Mass Spectrometry. *Environ Sci Technol* **36**, 7-11 (2002).

52 McConnell, J. R. & Edwards, R. Coal burning leaves toxic heavy metal legacy in the Arctic. *P Natl Acad Sci USA* **105**, 12140-12144 (2008).

53 Pasteris, D. R. *et al.* Seasonally resolved ice core records from West Antarctica indicate a sea ice source of sea-salt aerosol and a biomass burning source of ammonium. *J Geophys Res-Atmos* **119**, 9168-9182 (2014).

54 Abram, N. J., Mulvaney, R. & Arrowsmith, C. Environmental signals in a highly resolved ice core from James Ross Island, Antarctica. *J Geophys Res-Atmos* **116**, D20116, doi: 10.1029/2011jd016147 (2011).

55 Kaufmann, P. R. *et al.* An Improved Continuous Flow Analysis System for High-Resolution Field Measurements on Ice Cores. *Environ Sci Technol* **42**, 8044-8050 (2008).

56 Bigler, M. *et al.* Optimization of High-Resolution Continuous Flow Analysis for Transient Climate Signals in Ice Cores. *Environ Sci Technol* **45**, 4483-4489 (2011).

57 Ruth, U., Wagenbach, D., Steffensen, J. P. & Bigler, M. Continuous record of microparticle concentration and size distribution in the central Greenland NGRIP ice core during the last glacial period. *J Geophys Res-Atmos* **108**, doi: 10.1029/2002jd002376 (2003).

58 Woodruff, T. E., Welten, K. C., Caffee, M. W. & Nishiizumi, K. Interlaboratory comparison of Be-10 concentrations in two ice cores from Central West Antarctica. *Nucl Instrum Meth B* **294**, 77-80 (2013).

59 Berggren, A. M. *et al.* Variability of Be-10 and delta O-18 in snow pits from Greenland and a surface traverse from Antarctica. *Nucl Instrum Meth B* **294**, 568-572 (2013).

60 Bisiaux, M. M. *et al.* Changes in black carbon deposition to Antarctica from two high-resolution ice core records, 1850-2000 AD. *Atmos Chem Phys* **12**, 4107-4115 (2012).

61 Pasteris, D., McConnell, J. R., Edwards, R., Isaksson, E. & Albert, M. R. Acidity decline in Antarctic ice cores during the Little Ice Age linked to changes in atmospheric nitrate and sea salt concentrations. *J Geophys Res-Atmos* **119**, 5640-5652 (2014).

62 Rasmussen, S. O. *et al.* A first chronology for the North Greenland Eemian Ice Drilling (NEEM) ice core. *Clim Past* **9**, 2713-2730 (2013).

63 Coulter, S. E. *et al.* Holocene tephras highlight complexity of volcanic signals in Greenland ice cores. *J Geophys Res-Atmos* **117**, D21303, doi: 10.1029/2012jd017698 (2012).

64 Barbante, C. *et al.* Greenland ice core evidence of the 79 AD Vesuvius eruption. *Clim Past* **9**, 1221-1232 (2013).

65 Clausen, H. B. *et al.* A comparison of the volcanic records over the past 4000 years from the Greenland Ice Core Project and Dye 3 Greenland Ice Cores. *J Geophys Res-Oceans* **102**, 26707-26723 (1997).

66 Rolandi, G., Paone, A., Di Lascio, M. & Stefani, G. The 79 AD eruption of Somma: The relationship between the date of the eruption and the southeast tephra dispersion. *J Volcanol Geoth Res* **169**, 87-98 (2008).

67 Sun, C. Q. *et al.* Ash from Changbaishan Millennium eruption recorded in Greenland ice: Implications for determining the eruption's timing and impact. *Geophys Res Lett* **41**, 694-701 (2014).

68 Xu, J. D. *et al.* Climatic impact of the Millennium eruption of Changbaishan volcano in China: New insights from high-precision radiocarbon wiggle-match dating. *Geophys Res Lett* **40**, 54-59 (2013).

69 Deirmendjian, D. On volcanic and other particulate turbidity anomalies. *Advances in Geophysics* **16**, 267-296 (1973).

70 Vollmer, M. Effects of absorbing particles on coronas and glories. *Appl Optics* **44**, 5658-5666 (2005).

71 Sachs, A. J. & Hunger, H. Astronomical diaries and related texts from Babylonia. Volume 3: Diaries from 164 B.C. to 61 B.C. Wien: Verlag der Österreichischen Akademie der Wissenschaften (1996).

72 Wittmann, A. D. & Xu, Z. T. A Catalog of Sunspot Observations from 165 Bc to Ad 1684. *Astron Astrophys Sup* **70**, 83-94 (1987).

73 Rasmussen, S. O. *et al.* A new Greenland ice core chronology for the last glacial termination. *J Geophys Res-Atmos* **111**, D06102 doi: 10.1029/2005jd006079 (2006).

74 Herron, M. M., Herron, S. L. & Langway, C. C. Climatic Signal of Ice Melt Features in Southern Greenland. *Nature* **293**, 389-391 (1981).

75 Gao, C. H., Oman, L., Robock, A. & Stenchikov, G. L. Atmospheric volcanic loading derived from bipolar ice cores: Accounting for the spatial distribution of volcanic deposition. *J Geophys Res-Atmos* **112**, D09109, doi: 10.1029/2006jd007461 (2007).

76 Briffa, K. R. *et al.* Reassessing the evidence for tree-growth and inferred temperature change during the Common Era in Yamalia, northwest Siberia. *Quaternary Sci Rev* **72,** 83-107 (2013).

77 Grudd, H. Tornetrask tree-ring width and density AD 500-2004: a test of climatic sensitivity and a new 1500-year reconstruction of north Fennoscandian summers. *Clim Dynam* **31**, 843-857 (2008).

78 Salzer, M. W., Bunn, A. G., Graham, N. E. & Hughes, M. K. Five millennia of paleotemperature from tree-rings in the Great Basin, USA. *Clim Dynam* **42**, 1517-1526 (2014).

79 McMahon, S. M., Parker, G. G. & Miller, D. R. Evidence for a recent increase in forest growth. *P Natl Acad Sci USA* **107**, 3611-3615 (2010).

80 Salzer, M. W., Hughes, M. K., Bunn, A. G. & Kipfmueller, K. F. Recent unprecedented tree-ring growth in bristlecone pine at the highest elevations and possible causes. *P Natl Acad Sci USA* **106**, 20348-20353 (2009).

81 Briffa, K. R. *et al.* Reduced sensitivity of recent tree-growth to temperature at high northern latitudes. *Nature* **391**, 678-682 (1998).

82 Rohde, R. *et al.* A New Estimate of the Average Land Surface Temperature Spanning 1753 to 2011. *Geoinfor Geostat: An Overview* **1**, doi: 10.4172/2327-4581.1000101 (2013).

83 Mass, C. F. & Portman, D. A. Major volcanic eruptions and climate: A critical evaluation. *J. Climate* **2,** 566-593.

84 Fritts, H. C., Lofgren, G. R. & Gordon, G. A. Variations in Climate since 1602 as Reconstructed from Tree Rings. *Quaternary Res* **12**, 18-46 (1979).

85 Jensen, B. J. L. *et al.* Transatlantic distribution of the Alaskan White River Ash. *Geology* **42**, 875-878 (2014).

86 Oskarsson, N., Sigvaldason, G. E. & Steinthorsson, S. A Dynamic-Model of Rift-Zone Petrogenesis and the Regional Petrology of Iceland. *J Petrol* **23**, 28-74 (1982).

87 Kuehn, S. C., Froese, D. G., Shane, P. A. R. & Participants, I. I. The INTAV intercomparison of electron-beam microanalysis of glass by tephrochronology laboratories: Results and recommendations. *Quatern Int* **246**, 19-47 (2011).

88 Kaufman, D. S. *et al.* Late Quaternary tephrostratigraphy, Ahklun Mountains, SW Alaska. *J Quaternary Sci* **27**, 344-359 (2012).

89 Lakeman, T. R. *et al.* Holocene tephras in lake cores from northern British Columbia, Canada. *Can J Earth Sci* **45**, 935-947 (2008).

90 Bursik, M., Sieh, K. & Meltzner, A. Deposits of the most recent eruption in the Southern Mono Craters, California: Description, interpretation and implications for regional marker tephras. *J Volcanol Geoth Res* **275**, 114-131 (2014).

91 Sampson, D. E. & Cameron, K. L. The Geochemistry of the Inyo Volcanic Chain - Multiple Magma Systems in the Long Valley Region, Eastern California. *J Geophys Res-Solid* **92**, 10403-10421 (1987).

92 Veres, D. *et al.* The Antarctic ice core chronology (AICC2012): an optimized multi-parameter and multi-site dating approach for the last 120 thousand years. *Clim Past* **9**, 1733-1748 (2013).

93 Siebert, L., Simkin, T. & Kimberly, P. *Volcanoes of the World*. 3rd edn, University of California Press (2010).

Extended Data Figure 1 | Location of study sites. a) Map showing locations of the five ice-cores (WDC, B40, NEEM, NGRIP and TUNU) used in this study. Sites of temperature-limited tree-ring chronologies (green) [42,43,76-78] and sites with annual $\Delta^{14}C$ measurements from tree-rings in the 8th century CE (red outline) are marked; **b)** metadata for the ice cores, tree-ring chronologies and temperature reconstructions used.

Extended Data Figure 2 | Volcanic dust veils from historical documentary sources in relation to NEEM. Time series of 32 independently-selected chronological validation points from well-dated historical observations of atmospheric phenomena with known association to explosive volcanism (e.g., diminished sunlight, discolored solar disk, solar corona or Bishop's Ring, red volcanic sunset) as

reported in the Near East, Mediterranean region, and China, prior to our earliest chronological age marker at 536 CE. Black lines represent the magnitude (scale on vertical y-axes) of annual sulfate deposition measured in NEEM (NEEM and NEEM-2011-S1 ice cores) from explosive volcanic events on the new NS1-2011 timescale. Red crosses depict the 24 (75%) historical validation points for which NEEM volcanic events occur within a conservative ±3 year uncertainty margin. Blue crosses represent the eight points for which volcanic events are not observed. The association between validation points and volcanic events is statistically significantly non-random at >99.9% confidence.

Extended Data Figure 3 | Timescale comparison. Age differences of the timescales **a)** NS1-2011 and GICC05 for the NEEM-2011-S1/NEEM ice cores and **b)** WD2014 and WDC06A-7 for WDC. Differences before 86 CE (the bottom age of NEEM-2011-S1) deriving from the annual-layer counting of the NEEM core are shown for major volcanic eruptions relative to the respective signals in NGRIP on the annual-layer counted GICC05 timescale. Marker events used for constraining the annual-layer dating (solid line) and for chronology evaluation (dashed lines) are indicated. Triangles mark volcanic signals. Also indicated is the difference between WD2014 and the Antarctic ice-core chronology (AICC2012)[92], based on volcanic synchronization between the WDC and EDC96 ice cores.

Extended Data Figure 4 | Post-volcanic suppression of tree growth. Superposed epoch analysis for large volcanic eruptions using the **a)** 28 largest volcanic eruptions; **b)** 23 largest tropical eruptions; **c)** five largest NH eruptions; and **d)** eruptions larger than Tambora 1815 with respect to sulfate aerosol loading. Shown are growth anomalies of a multi-centennial tree-ring composite record (N-Tree) 15 years after the year of volcanic sulfate deposition, relative to the average of five years before the events. Dashed lines indicate 95% confidence intervals (2 SEM) of the tree-ring growth anomalies associated with the multiple eruptions.

Extended Data Figure 5 | Major element composition for ice core tephra QUB-1859 and reference material. Shown are selected geochemistry data: (**a)** SiO_2 vs. total alkali (K_2O + Na_2O); **b)** FeO (total iron oxides) vs. TiO_2; **c)** SiO_2 vs. Al_2O_3; and **d)** CaO vs. MgO) from 11 shards extracted from the NEEM-

2011-S1 ice core between 327.17 and 327.25 m depth, representing the age range 536.0–536.4 CE on the new, NS1-2011 timescale. Data for Late Holocene tephra from Mono Craters (California) are from the compilation by ref. 90 (all references in Methods); data for Aniakchak (Alaska) are from reference material published by ref. 88; and data for the early Holocene upper Finlay tephra , believed to be from the Edziza complex in the Upper Cordilleran Volcanic province (British Columbia), are from ref. 89.

Extended Data Table 1 | Ice-core dating. Parameters used for annual-layer interpretation. Parameters measured by the CFA system in the field are underlined. Stratigraphic age marker used to constrain annual-layer counting (*) and horizons used to evaluate the timescale (†).

Extended Data Table 2 | Annual-layer results using the StratiCounter program. Maximum-likelihood number of annual layers and confidence intervals derived from annual-layer counting between distinctive marker horizons and corresponding ages relative to the 775 CE ^{10}Be event.

*UE: Unattributed volcanic signal and year of sulfate deposition based on final age models (negative numbers are Year BCE).

†Year (BCE/CE) calculated from the number of annual layers relative to the fixed age marker in 775 CE.

‡Depth has been estimated from the average depth offset between NEEM-2011-S1 and NEEM.

§Fixed age marker based on the 10Be maximum annual value.

||Section with 6 m gap in the NEEM 2011-S1 core DRI data (this section is not used for calculating average age).

¶ This section is based on the NEEM field CFA data, since the DRI data does not cover the entire interval.

Section is based on combined data set of DRI and field-measured CFA data. The number of annual layers in this section from manual interpretation by investigator 1 was 383 (±7), and that of

862 investigator 2 was 393 (±8) layers. Most of the difference between the three layer counts was
863 occurring below 480 m (i.e., before 300 BCE), where data gaps were more frequent.
864 ☆Independent age markers used to constrain annual-layer dating in a second iteration to derive the
865 final ice-core age model NS1-2011.
866 **Tephra particles were extracted from the depth range 327.17–327.25 m depth (see
867 Supplementary Data).
868 ††Unattributed volcanic signal that was previously attributed to the historic 79 CE eruption of
869 Vesuvius[64].

870 **Extended Data Table 3 | Historical documentary evidence for key volcanic eruption age markers**
871 **536-939 CE.** A comprehensive list of all sources, including translations and assessment of the
872 confidence placed in each source and its chronological information is given in Supplementary Data.

873 **Extended Data Table 4 | Large volcanic eruptions during the past 2,500 years.** Years with negative
874 numbers are before the Common Era (BCE). Tentative attribution of ice-core signals to historic
875 volcanic eruptions is based on the Global Volcanism Program volcanic eruption database[93]. Average
876 (summer) temperature for the associated cold year is given for the average of Europe and the
877 Arctic[3].

878 *Total global aerosol forcing was estimated by scaling total sulfate flux from both polar ice sheets to
879 the reconstructed total (i.e., time integrated) aerosol forcing for Tambora 1815[7] (Methods); for high
880 latitude NH eruptions, Greenland fluxes were scaled by a factor of 0.57[6].
881 † Unattributed volcanic events (UE) and tentative attributions for non-documented historic
882 eruptions (?) are marked.

883 **Extended Data Table 5 | Post-volcanic cooling.** Coldest years and decades (1–2000 CE, JJA
884 temperature wrt. 1901–2000) for Europe[3] and years (500 BCE–1250 CE) and decades (500 BCE–2000
885 CE) with strong growth reduction in the N-Tree composite(wrt. 1000–1099). Ages of the volcanic

886 events from the ice cores reflect the start of volcanic sulfate deposition in Greenland (NS1-2011
887 timescale) with the largest 40 events indicated in bold letters and tropical eruptions underlined.
888 Years with negative numbers are before the Common Era (BCE).

889 * Latewood frost ring in bristlecone pines within ±1 year[34].

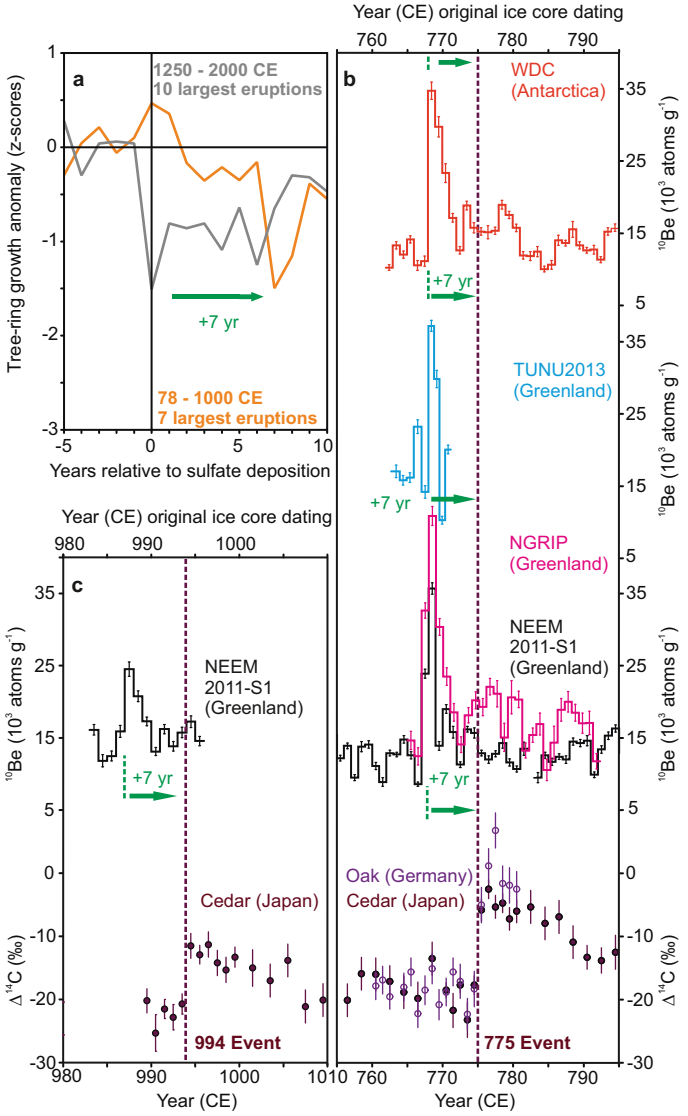
a
1250 - 2000 CE
10 largest eruptions
78 - 1000 CE
7 largest eruptions
+7 yr
Tree-ring growth anomaly (z-scores)
Years relative to sulfate deposition
b
Year (CE) original ice core dating
WDC
(Antarctica)
TUNU2013
(Greenland)
NGRIP
(Greenland)
NEEM
2011-S1
(Greenland)
Oak (Germany)
Cedar (Japan)
775 Event
c
NEEM
2011-S1
(Greenland)
Cedar (Japan)
994 Event
^{10}Be (10^3 atoms g^{-1})
Δ ^{14}C (‰)
Year (CE)

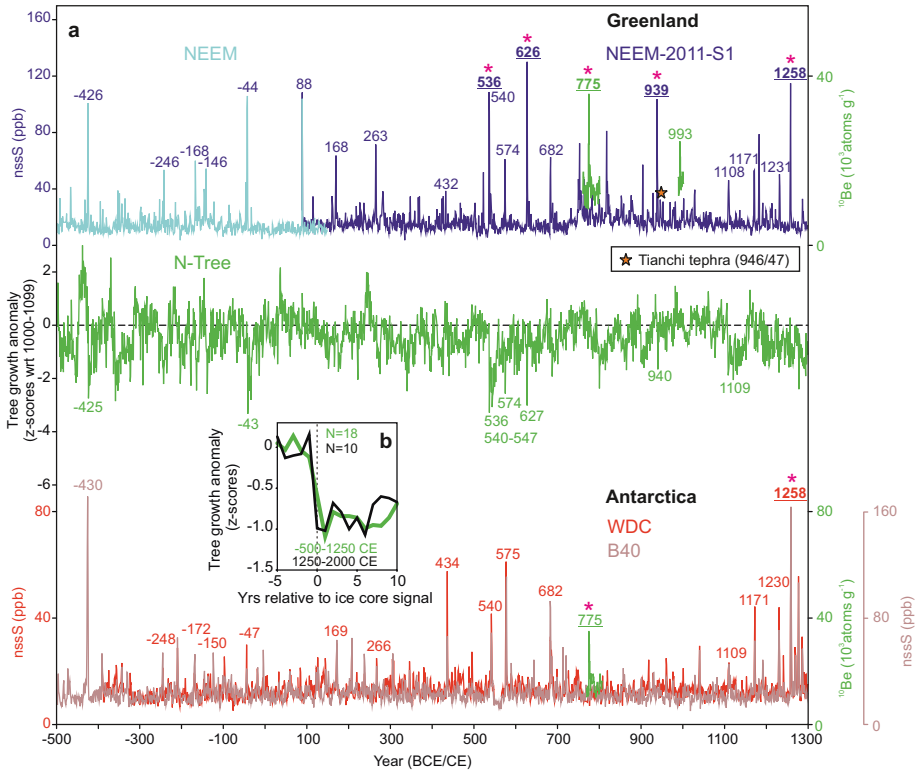
a
Greenland
NEEM
NEEM-2011-S1
nssS (ppb)
^{10}Be (10^3atoms g^{-1})
-426
-246
-168
-146
-44
88
168
263
432
536
540
626
574
682
775
939
993
1108
1171
1231
1258
Tianchi tephra (946/47)
N-Tree
Tree growth anomaly
(z-scores wrt 1000-1099)
-425
-43
536
540-547
574
627
940
1109
b
N=18
N=10
Tree growth anomaly
(z-scores)
-500-1250 CE
1250-2000 CE
Yrs relative to ice core signal
Antarctica
WDC
B40
-430
-248
-172
-150
-47
169
266
434
540
575
682
775
1109
1171
1230
1258
nssS (ppb)
^{10}Be (10^3atoms g^{-1})
Year (BCE/CE)

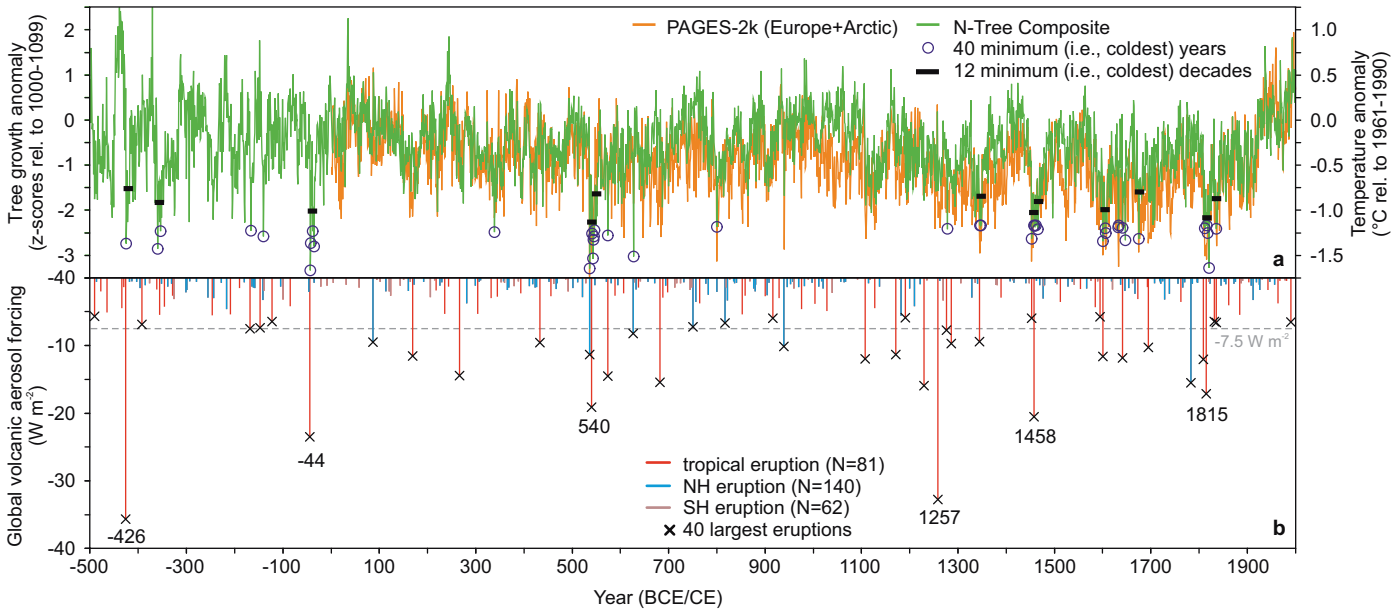
PAGES-2k (Europe+Arctic)
N-Tree Composite
40 minimum (i.e., coldest) years
12 minimum (i.e., coldest) decades
Tree growth anomaly (z-scores rel. to 1000-1099)
Temperature anomaly (°C rel. to 1961-1990)
a
-7.5 W m-2
-426
-44
540
1257
1458
1815
tropical eruption (N=81)
NH eruption (N=140)
SH eruption (N=62)
40 largest eruptions
Global volcanic aerosol forcing (W m-2)
b
Year (BCE/CE)

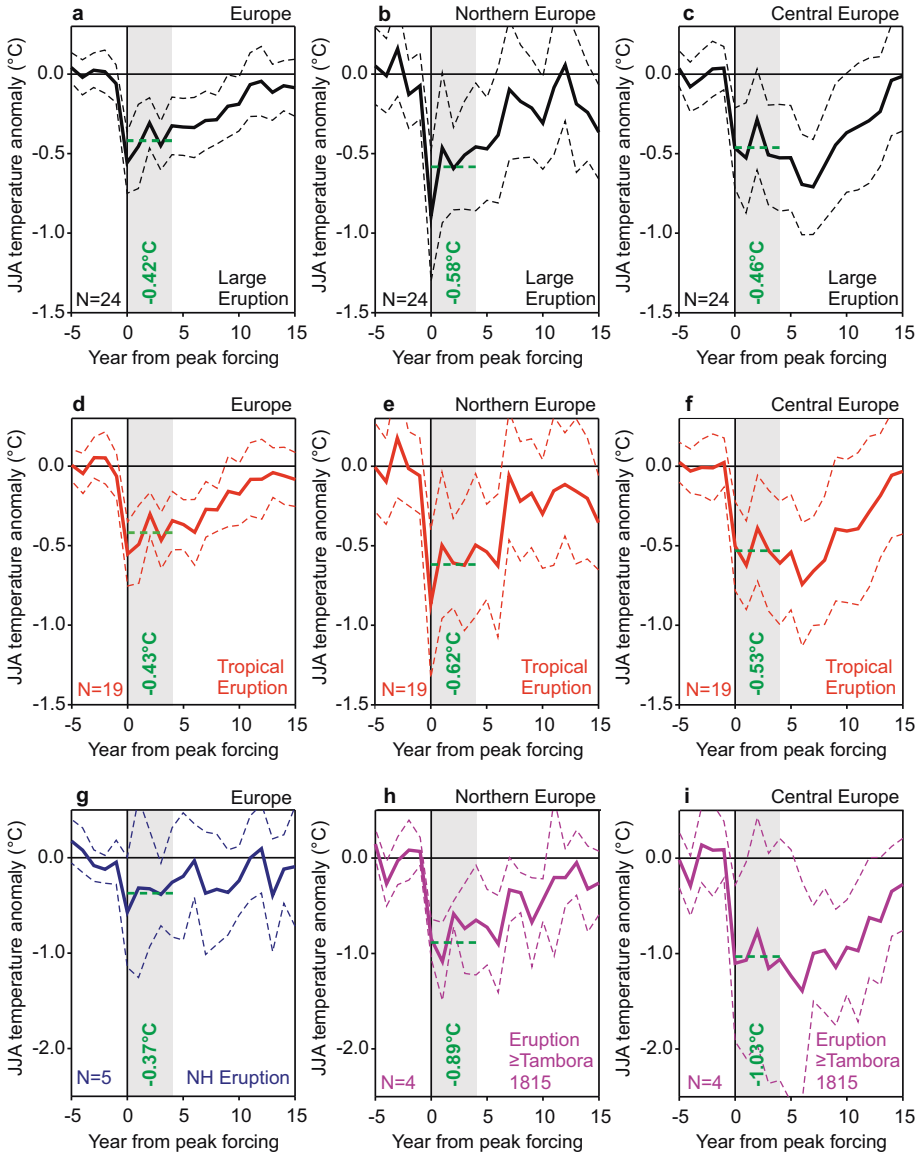
a
Europe
b
Northern Europe
c
Central Europe
d
Europe
e
Northern Europe
f
Central Europe
g
Europe
h
Northern Europe
i
Central Europe
JJA temperature anomaly (°C)
Year from peak forcing
N=24
-0.42°C
Large Eruption
N=24
-0.58°C
Large Eruption
N=24
-0.46°C
Large Eruption
N=19
-0.43°C
Tropical Eruption
N=19
-0.62°C
Tropical Eruption
N=19
-0.53°C
Tropical Eruption
N=5
-0.37°C
NH Eruption
N=4
-0.89°C
Eruption ≥Tambora 1815
N=4
-1.03°C
Eruption ≥Tambora 1815

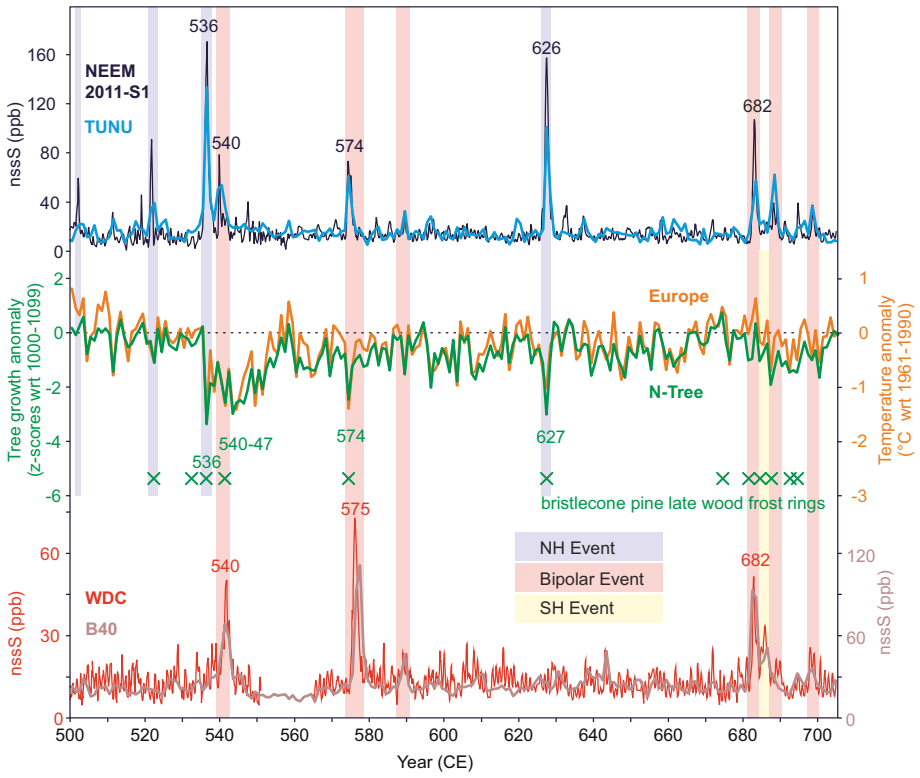
NEEM
2011-S1
TUNU
nssS (ppb)
536
540
574
626
682
Europe
N-Tree
Tree growth anomaly
(z-scores wrt 1000-1099)
Temperature anomaly
(°C wrt 1961-1990)
540-47
627
bristlecone pine late wood frost rings
575
NH Event
Bipolar Event
SH Event
WDC
B40
Year (CE)